Effects of light / dark diel cycles on the photoorganoheterotrophic metabolism of *Rhodopseudomonas palustris* for differential electron allocation to PHAs and H_2

Marta Cerruti[a], Heleen T. Ouboter[a,*], Viktor Chasna[a], Mark C. M. van Loosdrecht[a], Cristian Picioreanu[a], David G. Weissbrodt[a,#]

[a] Department of Biotechnology, Delft University of Technology, Delft, The Netherlands

[#] Correspondence to: David G. Weissbrodt (d.g.weissbrodt@tudelft.nl)

[*] Present address: Heleen T. Ouboter, Department of Microbiology, Radboud University Nijmegen, Nijmegen, The Netherlands

E-mail addresses: m.cerruti@tudelft.nl; h.ouboter@science.ru.nl; v.chasna@student.tudelft.nl; m.c.m.vanloosdrecht@tudelft.nl; c.picioreanu@tudelft.nl; d.g.weissbrodt@tudelft.nl

Running title: *Rhodopseudomonas* metabolism under light/dark cycles

Word counts: Abstract: 250 words; Importance: 150 words; Manuscript: 5060 words

Abstract

Light/dark cycles can impact the electron distribution in *Rhodopseudomonas palustris*, a hyperversatile photoorganoheterotrophic purple non-sulfur bacterium (PNSB). Dynamic conditions during diel cycles are important for the physiology of PNSB, but the coupling between illumination patterns and redox balancing has not been extensively studied. For survival and growth, *Rhodopseudomonas* has developed different mechanisms to allocate electrons under dynamic growth conditions. Products such as hydrogen and poly-β-hydroxyalkanoates (PHAs) can form alternative electron sinks. A continuous culture, fed with a balanced nutrients medium, was exposed to three different conditions: 24 h continuous infrared illumination, 16h light/8h dark, and 8h light/16h dark. Light and dark phase durations in a cycle determined the energy availability level (light) and the attainment of a stationary state. Under long dark phases, the acetate substrate accumulated to levels that could not be depleted by growth in the light. Under short dark phases, acetate was rapidly consumed in the light with most of the phototrophic growth occurring under acetate-limiting conditions. Under diel cycles, substrate uptake and growth were unbalanced and *Rhodopseudomonas* shunted the excess of carbon and electron flow first toward PHAs production. Only secondarily, when PHA storage got saturated, the electron excess was redirected toward H_2. A numerical model described well the dynamics of biomass and nutrients during the different light/dark cycle regimes. The model simulations allowed determination of stoichiometric and kinetic parameters for conversion by *Rhodopseudomonas*. Understanding the inherent process dynamics of diel light cycles in purple sulfur bacteria cultures would enable optimization procedures for targeted bioproduct formation.

Importance

Purple non-sulfur bacteria (PNSB) are important anoxygenic phototrophic microorganisms that take part in numerous environmental processes, based on their metabolic versatility. *Rhodopseudomonas*

palustris is a model photosynthetic bacterium of the PNSB guild. Light cycles influence deeply its physiology. Poly-β-hydroxyalkanoates (PHAs) and biohydrogen are two of the most studied metabolic products of *Rhodopseudomonas*, because of their biotechnology potential besides involvement in carbon and electron allocations in its metabolism. Their production mechanisms have often been described as competitive, but the rationale behind the production of one or the other compound has not been elucidated. Here, we found that under light / dark cycles an excess of organic substrate was first directed toward PHAs production, and only when this pathway was saturated H_2 was produced. Understanding the dynamics of carbon and electron allocation under intermittent light cycles enhances our knowledge on PNSB metabolisms and paves ways to manage the formation of targeted bioproducts.

Keywords

purple non-sulfur bacteria; photoorganoheterotrophy; electron distribution; biohydrogen; polyhydroxyalkanoates; diel cycles; mathematical modeling

Introduction

Purple non-sulfur phototrophic bacteria (PNSB) form a guild of hyper-versatile anoxygenic phototrophs (1), able to grow on different organic and inorganic substrates (2). *Rhodopseudomonas palustris* is one model PNSB (3). It can produce compounds of industrial interest, such as single cell proteins (4), carotenoids (5), hydrogen gas (H_2; used as biofuel) and poly-β-hydroxyalkanoates (PHAs; used as bioplastics) (6,7). Under light and in presence of organic carbon, *Rhodopseudomonas* grows photoorganoheterotrophically even in absence of external electron acceptors. Under dark, growth is possible on sugars with external electron acceptors (as nitrate, trimethylamine-N-oxide or dimethyl sulfoxide) (8,9).

Light is crucial for phototrophy by providing energy to cells. PNSB capture the photonic energy and couple the light-driven oxidation of the photopigments to an electron transfer through membrane bound-enzymes. The trans-membrane gradient of hydrogen protons (H^+) supports ATP synthesis through cyclic photophosphorylation (10). NADH is mainly produced during catabolic processes. In some cases, a reverse electron flow takes places, and the NADH-dehydrogenase catalyze the proton transfer from the ubiquinone pool to NAD^+. The control of redox balance is crucial for cell survival and growth. The ratio between NADH/NAD^+ is important for intracellular redox homeostasis (11). PNSB generate NADH in three different ways (Figure 1), namely: 1) anabolic processes (12), 2) light driven reactions through the quinone pool (1); 3) reverse electron transfer (13).

To cope with possible redox imbalances, mainly arising in anabolic processes, PNSB redistribute the electrons toward different routes (14). In *Rhodopseudomonas*, the first and most important electron sink is the biomass itself, that receives the intermediates of the tricarboxylic acid cycle and the NADPH produced there (15). Secondly, the Calvin-Benson-Bassham (CBB) cycle is constitutively active also under photoorganoheterotrophy as central recycling mechanism of redox

cofactors coming from the anabolic process (15,16). Under photoorganoheterotrophic anaerobic conditions, a surplus of electrons can be disposed through PHA or H_2 production. Both electron sinks are normally produced under nitrogen limitation. Nitrogenase-mediated H_2 production has been extensively described (1). H_2 is a side-product of the nitrogen fixation process, that can only happen when no preferred nitrogen source like ammonium or glutamate is available (17–19). Hydrogenase-mediated H_2 production has been reported in presence of an oxidized organic compound (*i.e.* malate) (21). Several bacterial species accumulate PHAs in the cells as a mean of carbon and electrons storage under normal conditions (22). In lab-scale experiments, to achieve an over production, these storage polymers are synthetized when acetyl-CoA and NADPH are in excess but nutrients like nitrogen, sulfur or phosphorus are limiting (23). Similar to other bacteria, PNSB can produce PHAs (24) as a mean of carbon and electron balance, utilizing the reducing power to build the storage polymers (25,26). PHAs production in PNSB occurs under balanced growth, and it increases under nutrient limitations (27). The two processes of H_2 and PHA production are considered competitive electron dissipation pathways (28,29). However, the hyper-versatility of PNSB metabolisms has not enabled to identify an univocal response to redox imbalances.

In natural environments, phototrophs are subjected to diel (*i.e.*, 24-h period) light / dark cycles. Since light is responsible for the production of energy and reducing power, the irradiation patterns impacts the cellular physiology. The light and dark cycles impact cells redox and ATP balance, subjecting cells to metabolic switches. How it affects the internal electron allocation patters and how PNSB respond to these switches remains puzzling. Allocation of reducing power toward the aforementioned routes is known, but mechanisms that govern the preferential electron flow have not been explained.

111 Here, we aimed to elucidate the effects of diel light / dark cycles on the physiology and electron
112 allocation in *Rhodopseudomonas palustris*, isolated from an in-house PNSB enrichment culture for
113 nutrient removal from wastewater (30). The dynamic conditions were hypothesized to influence the
114 physiology of purple bacteria, as the energy source is intermittently provided. The process mimics a
115 potential natural scenario, where day and night cycles are applied and create a redox imbalance. We
116 elucidated the preferential carbon and electron redistribution toward the most important competitive
117 pathways of PHAs and H_2 formation during diel light / dark cycles.
118

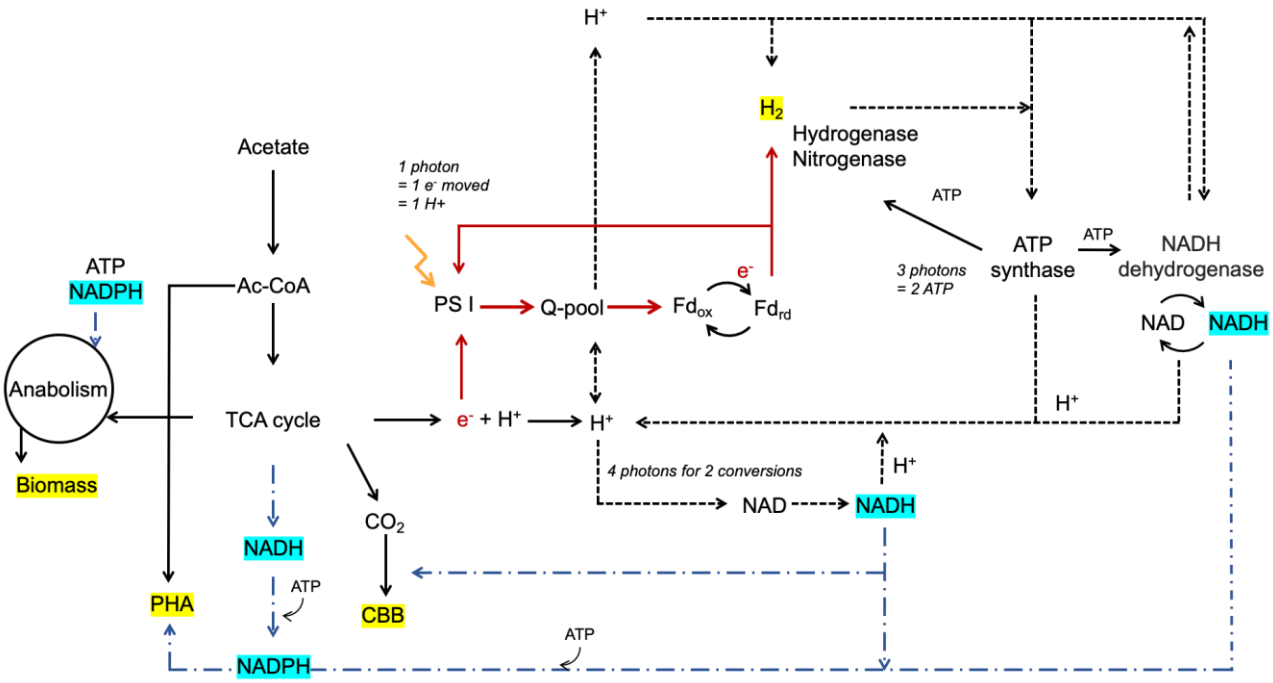

119

120 **Figure 1.** Schematic representation of the reducing power allocation in *Rhodopseudomonas*. Red lines: electron flow;
121 Black dashed lines: proton transfer; Blue dotted lines: NADH is normally produced in the catabolic processes, whereas
122 NADPH is used in the anabolic processes, such as PHAs formation. Biomass and CBB are the primary electron sinks in
123 PNSB. PHAs and H_2 are two of the other possible electron sinks.

124

Results

Three regimes for continuous cultivation of *Rhodopseudomonas palustris* were tested: continuous illumination, cyclic 16 h light / 8 h dark, and cyclic 8 h light / 16 h dark. The biomass and CO_2 yields (Y_{XS} and Y_{CX}) and the maximum biomass-specific growth rate (μ_{max}) were estimated using data from the 16 h light / 8 h dark experiment (Table 1). The calibrated model was used to predict the behavior of the 8 h light / 16 h dark cycles.

Biomass production of *Rhodopseudomonas palustris*

Under continuous illumination, the biomass reached a constant concentration of 12.10 ± 0.44 C-mmol L^{-1}, corresponding to 88% of carbon or 99% of reduction equivalents (COD) provided in the influent. Around 11% of the carbon present in the inflow was recovered as CO_2 (0.112 C-mmol L^{-1}) in the off-gas. HPLC results showed no residual acetate in the bulk liquid at steady state.

Under cyclic operations (Figure 2), the system reached a stable behavior with similar changes in concentrations during each cycle. Within a cycle a clear dynamic pattern was observed. Under dark, the biomass did not grow and was only washed-out. The biomass wash-out rate ($F/V \cdot C_X$) was very well represented by the numerical model (Figure 2A,B). The corresponding change in acetate, ammonium and phosphate concentrations during the dark phases matched with the expected change based on the feeding rate. No conversion occurred in the dark.

Under 16-h light, the biomass accumulation exceeded the dilution rate $D=F/V$. An initial growth rate (assumed to be μ_{max}) of 0.15 h^{-1} was observed, and reached a steady value ($\mu = D = 0.04$ h^{-1}) after 2 h exposed to light (Figure 2A). The acetate concentration reached a minimal steady value when the biomass growth rate achieved the steady state.

Under shorter 8-h light periods, the biomass growth rate did not reach a stationary-state in a cycle, being around 0.1 h^{-1}. Acetate was not depleted at the end of the light phase (Figure 2B). The biomass increase changed from 11 C-mmol L^{-1} on first cycle to 5 C-mmol L^{-1} on fourth cycle. The growth rate μ during the 8 h light period was approximately 0.12 h^{-1} thus lower than the μ_{max}. The estimated biomass yield on acetate in the light was 0.88 C-mol X C-mol^{-1} acetate for both the 16 h light and the 8 h light phases, equal to the yield in continuous light regime.

Table 1. Model parameters. The maximum biomass-specific growth rate and yields were fitted to experimental data, while the other parameters were measured during experiments, calculated or obtained from literature.

Parameter name	Symbol	Value	Units	Source
Max. biomass-specific growth rate	μ_{max}	0.15	C-mol X · h^{-1} · C-mol^{-1} X	Fitted
Biomass yield	Y_{XS}	0.88	C-mol X · C-mol^{-1} S	Fitted
Ammonium yield	Y_{NX}	0.18	mol · C-mol^{-1} X	Fitted
Phosphate yield	Y_{PX}	0.009	mol · C-mol^{-1} X	Fitted
CO_2 yield	Y_{CX}	0.142	mol · C-mol^{-1} X	Fitted
Reactor radius	R	0.055	m	Measured
Liquid volume	V	1.2	L	Measured
Liquid flow rate	F	0.048	L·h^{-1}	Measured
Dilution rate	D	0.04	h^{-1}	F/V
Gas volume	V_g	0.3	L	Measured
Gas flow rate	F_g	7.14	L·h^{-1}	Measured
Inflow acetate concentration	$C_{S,in}$	7	mM	Measured
Inflow ammonium concentration	$C_{N,in}$	4.28	mM	Measured
Inflow phosphate concentration	$C_{P,in}$	0.22	mM	Measured
Light intensity at reactor walls	I_0	300	W·m^{-2}	Measured
Light extinction coefficient per biomass concentration	ε	0.1	m^2·g^{-1}	(17)
Half-saturation coefficient acetate	K_S	0.1	mM	Lower than

				in (36) (0.3 mM)
Half-saturation coefficient ammonium	K_N	0.001	mM	(37)
Half-saturation coefficient phosphate	K_P	0.003	mM	(38)
Half-saturation coefficient light	K_I	10	$W \cdot m^{-2}$	(39)
CO_2 mass transfer coefficient	k_La	32	h^{-1}	Calculated (SI-1)
Henry coefficient CO_2	H_C	0.03 (at 30°C) 0.04 (at 20°C)	$mol \cdot L^{-1} \cdot atm^{-1}$	(40)

Carbon, nitrogen and phosphorus assimilation

Under continuous illumination, no residual acetate was detected in the bulk liquid. Under 16 h light, acetate was almost fully depleted, down to a concentration around 1 C-mmol L^{-1}, as also very well represented by the numerical model. Under 8 h light, acetate was still present in the bulk liquid in concentrations ranging from 4 to 1.5 C-mmol L^{-1}. In this case, the model overestimates the rate of acetate consumption, *i.e.* predicting acetate depletion at the end of the light phase.

Nitrogen and phosphorus sources were provided in excess, and never became limiting. Under light, N and P were consumed, resulting in a decrease in their concentrations (Figure 2C,D). Under dark, the fed N and P accumulated since not assimilated in biomass. At the end of the dark phase, 3.6 ± 0.6 N-mmol L^{-1} and 0.14 ± 0.01 P-mmol L^{-1} remained the bulk liquid. N and P dynamics showed irregular behaviour under 16 h light (Figure 2C). Therefore, the Y_{NX} and Y_{PX} were fitted on the 8 h light experiment (Figure 2D). The determined yields (Y_{NX} = 0.18, Y_{PX} = 0.009) were very close to the theoretical yields resulting from considering the biomass elemental composition (Y_{NX} = 0.18, Y_{PX} = 0.014) measured in (35). With these yields, the N and P dynamics during the 8 h light cycles were well represented by the model: accumulation under dark and consumption under light.

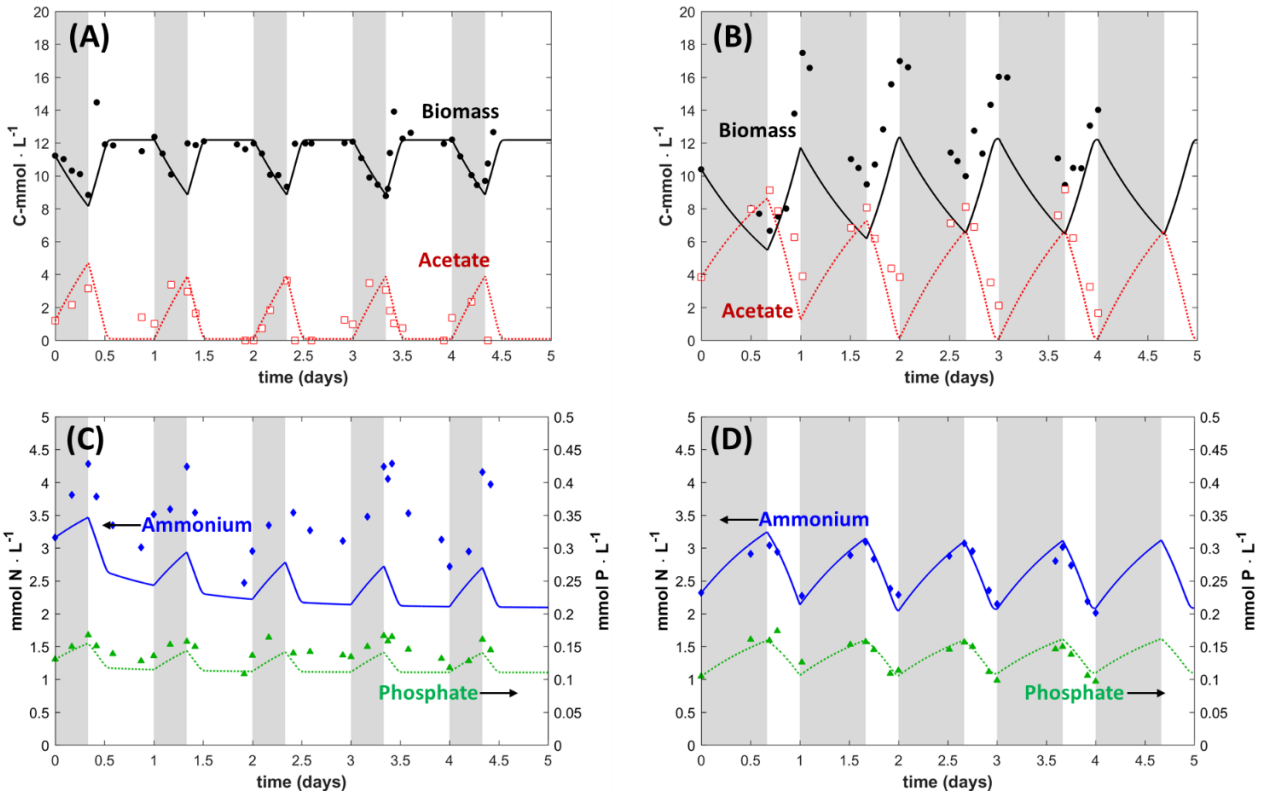

Figure 2. Dynamics of biomass, acetate, ammonium and phosphate concentrations during light-dark cycles: (A),(C) 16 h light / 8 h dark; (B),(D) 8 h light / 16 h dark. Gray areas represent the dark periods. (A),(B) biomass (black circles) and acetate (red open squares) measured concentrations, with lines being the model results. The biomass concentration achieved a stationary state, while acetate reached very low (limiting) concentrations after 2 h of the 16 h light periods. The biomass increased without reaching a steady state during the 8 h light periods, while acetate was not fully consumed. (C),(D) ammonium (blue diamonds) and phosphate (green triangles) measured concentrations, with lines being the model results. Concentrations of N and P were not limiting for the system in any illumination phase.

CO_2 production follows the biomass growth patterns

The CO_2 production rate was constant at 0.075 ± 0.001 mmol h^{-1} during continuous illumination (Figure 3A): the chemostat achieved a stationary operation. Under light/dark cycles, CO_2 emission in the off-gas decreased in the dark to 0.03 mmol h^{-1} (Figure 3B). Possibly, the registered baseline value can be due to the detection limit of the MS instrument. Under 16 h light, CO_2 emission increased rapidly within the first hour, reaching 0.25 mmol h^{-1}, following the biomass growth rate with acetate uptake. Once the acetate reached the minimal level, the CO_2 production also decreased

to a stable level of 0.07 mmol h^{-1} after the second hour of illumination, reflecting the steady state operation. The numerical model reproduced the observed trends during light phase, but the residual CO_2 production in the dark phase was not accounted for.

Under 8 h light / 16 h dar, the CO_2 production did not achieve a steady state. In the light phase, the CO_2 production increased with 0.05 to 0.08 mmol h^{-1} during the cycles, reaching a peak after 4 h (0.88 ± 0.013 mmol h^{-1}), which was described only qualitatively by the model (Figure 3C). The reason for the discrepancy between model and experimental data is the larger computed acetate consumption rate, which leads to a higher CO_2 formation rate in the model results. In both illumination regimes, the CO_2 production dropped to the same stable value of 0.033 mmol h^{-1} during the dark phase.

H_2 is produced only during the short light periods

A very low H_2 production was recorded during the continuous illumination with rates of around 0.004 mmol h^{-1} (Figure 3D). Occasionally, unexplained H_2 spikes were recorded. During the 16 h light experiment, dark-phases hydrogen production was negligible and no specific production pattern was measured in the light (Figure 3E). The very low H_2 concentration may relate to an instrumental offset. However, H_2 was produced constantly during the 8 h light periods (Figure 3F), with an increase of 0.02 ± 0.01 mmol h^{-1} per cycle and reaching a maximum of 0.05 mmol h^{-1}. The biomass-specific rate of H_2 production under 8 h light was 10 times higher (0.156 mmol H_2 h^{-1} g^{-1} DW) than under all other conditions (0.014 mmol H_2 h^{-1} g^{-1} DW).

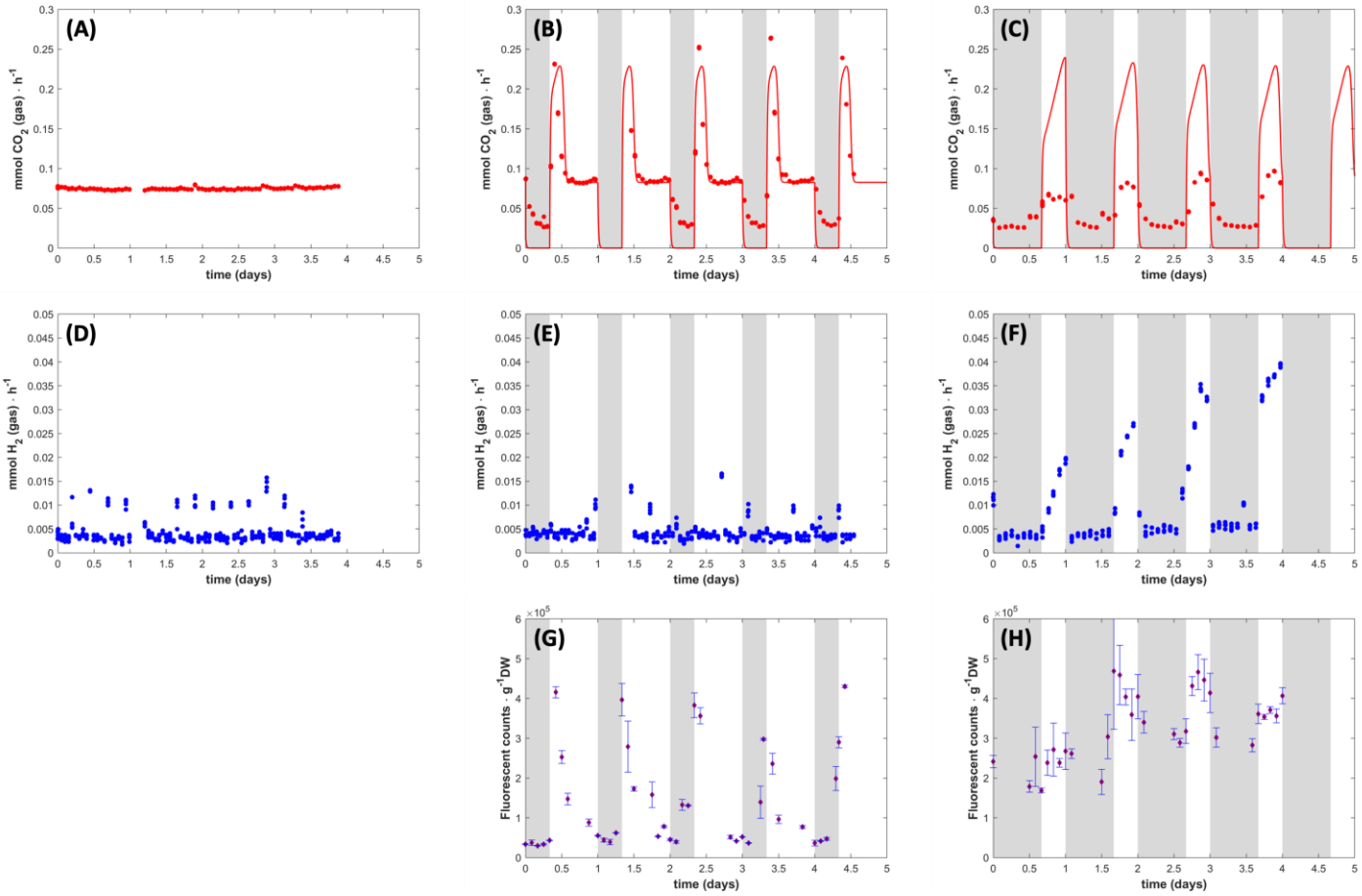

Figure 3. Dynamics of CO_2, H_2 and PHA during light-dark cycles: (A),(D) continuous illumination; (B),(E),(G) 16 h light / 8 h dark; (C),(F),(H) 8 h light / 16 h dark. Gray areas represent the dark periods. (A),(B),(C) CO_2 production rate - measured (red circles) and computed (lines). CO_2 production was constant during continuous illumination, but peaks appeared during light-dark cycles, correlated with the acetate uptake. (D),(E),(F) measured H_2 production (blue circles). Constant low level H_2 was produced during continuous illumination and 16 h light cycles, but H_2 production strongly increased in each light period of the 8 h light cycles. (G),(H) PHAs fluorescent counts per gram biomass in the light/dark experiments. A PHAs peak was measured at the beginning of each of the 16 h light phases, however less clear pattern could be detected under 8 h light.

PHA production follows CO_2 formation under 16 h light but not under 8 h light

Due to the low biomass concentration, a traditional PHA extraction and GC quantification (41) was not possible. Fluorimetry was used to detect PHAs in the biomass, giving a relative quantification (34). PHAs were not detectable under continuous illumination. A fluorescence count peak was detectable after 2 h from the light switch in the 16-h light phases ($3.8 \pm 0.5 \cdot 10^5$ fluorescent counts g-

^{1} DW) (Figure 3G), concomitantly to the peak of CO_2 production. The PHAs decreased constantly after the peak, reaching a baseline at $3 \cdot 10^4$ fluorescent counts g^{-1} DW. Under 8 h light / 16 h dark cycles (Figure 3H), PHA production during light was less pronounced. More PHAs were detectable in the dark compared to the 16 h light regime. These observations indicate that the diel light regimes induced PHA formation, with the long light regime generating a typical feast-famine behavior (42), while the short light regime stimulated a higher PHAs content in the cells.

Discussion

Acetate rather than light drives the metabolic responses of *Rhodopseudomonas*

Light energy source is central for the catabolic processes in PNSB. Organic substrates are used as C-source for biomass synthesis and as electron donors. When no external electron acceptor is present, the difference in degree of reduction between substrate and biomass has to be balanced with internal electron reallocation processes. The dynamics of the change in N and P concentrations were congruent with the biomass formation and their measured yields were close to the elemental biomass composition ($CH_{1.8}O_{0.38}N_{0.18}P_{0.014}$) determined in another study (35). Carbon balances closed for the continuous illumination experiment and for the 16 h light / 8 h dark experiment, but not for the 8 h light / 16 h dark cycles, where the C-balances seemed to indicate a net production (Table 2). PHA granules that were always present in the cells under 8 h light / 16 h dark may have led to an absorbance overestimation of the biomass present in the reactor.

Table 2. Distribution of the carbon sources and carbon balances under different illumination conditions

Light/dark regimes	**Carbon inputs (C-mmol h^{-1})**	**Carbon outputs (C-mmol h^{-1})**				**Carbon balance (% C)**	**Electron balance (% COD)**
Component	Acetate	Acetate	Biomass	CO_2	Σ out		
Phase	Influent	Effluent	Effluent	Off-gas			
24 h light	0.66±0.05	<LOD[1]	0.58	0.07±0.001	0.65	98%	98%
16 h light	0.66±0.05	0.11±0.01	0.57±0.01	0.08±0.01	0.75±0.01	115±2%	113±1%
8 h dark		0.10±0.02	0.51±0.03	0.07±0.02	0.68±0.06	103±9%	102±9%
8 h light	0.61±0.006	0.28±0.03	0.62±0.05	0.07±0.01	0.97±0.05	158±8%*	159±9%*
16 h dark		0.19±0.07	0.57±0.12	0.03±0.002	0.79±0.15	130±25%*	137±27%*

[1]limit of detection; * the overvaluation of the carbon and electron balance can be due to an overestimation of the biomass concentration. The absorbance measures taken might have influenced by the presence of PHAs inside the cells.

Light / dark cycles occur daily in natural environments. Phototrophic organisms have adapted to

cope with imbalances in energy supply. Purple bacteria have higher biomass production under light / dark cycles (43,44). H_2 production is increased under discontinuous illumination, following the biomass trend (45,46).

Here, the light cycles are important not only for the energy that light provides, but most importantly for the time available for the cultures to metabolize the nutrients. The light intensity at the surface of the reactor was 300 W m^{-2}. Considering the attenuation due to the biomass concentration and the reactor depth, the minimum calculated light available was 180 W m^{-2} (Figure SI-4). Under any given condition, the available light intensity was not limiting the microbial metabolism since always exceeding the half-saturation coefficient for light, defined at K_i =10 W m^{-2} (39). Purple bacteria adapt the number and type of photosynthetic unit components based on the different light intensities (47), but Imam et al. (48) reported that light may be saturating for PNSB growth already at 100 W m^{-2}. We can therefore assume that the irradiance intensity used in our study during the light periods did not deeply affect the metabolic state of the cells.

The continuous cultivation system was initially set-up based on the stoichiometric and kinetic parameters derived from batch experiments. In the continuously illuminated chemostat, the biomass reached a steady-state, acetate was limiting (i.e., low concentrations), and the biomass growth rate equaled to the dilution rate (0.04 h^{-1}). Once the light/dark cycles were applied, a disturbance of the steady-state was immediately observed. Under long (16 h) illumination, the biomass consumed the acetate for growth and after an initial increase of the growth rate the steady-state conditions were restored for the remaining two thirds of the light cycles (with a specific growth rate again equal to the dilution rate). Longer (16 h) dark periods led to an increased accumulation of acetate in the bulk liquid (twice as high as in the 8 h dark), since acetate was fed twice longer and there was no consumption in the dark. Due to the shorter light (8 h light) periods, acetate was not fully consumed at the end of the light phases. Therefore, acetate was no more the growth rate limiting compound

and the light period was too short to reach a steady state. The growth rate in the light phase exceeded the value of the imposed dilution rate, leading to a transient accumulation of biomass (Figure 2B). The modelled biomass dynamics agreed with the measurements, fitting quantitatively the values for the 16 h light experiment, where the exact steady state values were obtained. When using the same model parameters for the short (8 h) illumination experiment, the calculated amount of biomass formed during the light periods corresponded well to the values measured only for the second and later cycles, while for the first cycle the model underestimated the biomass formed. The disagreement may be related to the carbon imbalance reported in Table 3. Still, given longer illumination in the last model cycle would allow the biomass to reach exactly the same steady state as in the longer light period experiment (Figure SI-3) after about 10 h light and acetate attained the minimum.

The average acetate consumption rates under 16 h light were 0.08 C-mol h^{-1} L^{-1} (Figure SI-5) and under 8 h light were 0.15 C-mol h^{-1} L^{-1} (Figure SI-6). Initially, the biomass grew at the maximum substrate uptake rate. If the light phase was too short (as in the 8 h light periods), acetate was not fully consumed (2.5 ± 1.1 C-mmol L^{-1}) and the biomass grew at its maximum growth rate.

PHA synthesis patterns reflect the metabolic state of the cells

PHAs can be formed under dynamic conditions or because of imbalance in the degree of reduction between biomass and carbon source. PHAs constitute carbon and energy stocks (49,50). In chemostat conditions, carbon was continuously fed to the cultures and cells did not store PHAs. PHA synthesis in purple bacteria has primarily been reported under nitrogen limitation, as an intrinsic mechanism for the redistribution of carbon excess. PHA accumulation is conventionally reported under growth-limiting conditions (51,52) when the carbon sources are available, but the nutrients (such as N, P or S) to produce cellular components are limited resulting in acetyl-CoA accumulation in the cells.

307

308 During the anabolic reactions, *Rhodopseudomonas* incorporates acetate in the form of acetyl-CoA
309 and releases at the same time CoA. In highly active cells, the levels of acetyl-CoA are low, but the
310 levels of CoA are high. In contrast, in non-growing cells, acetyl-CoA is not utilized in anabolic
311 processes and accumulates in the cells (53). A high acetyl-CoA to CoA ratio and the presence of
312 NADPH are required for the initiation of the PHA pathway (54).

313

314 The ratio between carbon sources and other nutrients is important to maintain the balance between
315 substrate uptake rate and growth rate. The inflow was defined based on the biomass composition of
316 purple bacteria (38), with a C:N ratio of 5.68:1 mol/mol was used in the medium. Nitrogen was
317 provided in excess preventing N-limitation imbalance. Consequently, under continuous
318 illumination, no production of PHAs was detected.

319

320 After a period of darkness, the biomass was subjected to an excess of light and nutrients (acetate,
321 ammonium, phosphate) resulting in an increased substrate uptake rate. For the first 2 h after
322 switching on the 16-h light phase, the growth rate was close to the previously measured maximal
323 growth rate μ_{max} of 0.15 h^{-1}. After 3 h, when acetate was no more in excess, the growth rate
324 stabilized again at the dilution rate value of 0.04 h^{-1}. When shorter (8 h) light periods were applied,
325 the initial growth rate was ~0.1 h^{-1}. Under both conditions, cells exhibited growth rates close to
326 μ_{max}. This resulted in the production of reducing power, which, along with the NADH produced in
327 the photosynthetic processes, became in excess and had to be reallocated. As reported by Kanno et
328 al. (55), the photosynthetic units are not disassembled in the dark, even under starvation. These are
329 readily available, once the light conditions are restored, to produce ATP and NADH for the
330 biosynthetic processes. This, linked to the prompt availability of the enzymes for PHAs formation
331 that are constitutively expressed (56), leads to the immediate production of PHAs. Under 16 h light,
332 a peak of fluorescent counts was observed 2 h after the light switch, but it decreased to baseline

333 levels (steady state) once the growth rate stabilized again at 0.04 h^{-1}. The fluorescent counts
334 decreased and no H_2 production was observed. Cells reached a maximal capacity of substrate
335 uptake, though not coupled to a maximal growth rate, similarly to what is described in (57).
336
337 Under 8 h light / 16 h dark cycles, acetate was not completely consumed during illumination and
338 increasingly accumulated during the dark phases, resulting in a further imbalance in the redox state
339 of the cells. The redox imbalance generated by the continuous presence of acetate, rather than the
340 illumination conditions alone, led to a more constant production of PHAs. The cells were highly
341 active, with a growth rate close to the maximal growth rate, leading to a low availability of CoA
342 that resulted in PHAs formation. Only when the PHAs pool got saturated the NADPH pool was
343 further increased, and H_2 production became possible.
344
345 **H_2 production is a secondary pathway of electron dissipation**
346 The H_2 production rates here reported are low compared to other studies that have exposed PNSB to
347 similar light intensities (48). However, our experimental conditions were not designed to stimulate
348 H_2 production. H_2 can be produced either via the nitrogenase system, either via the ferredoxin-
349 hydrogenase system. Ammonium is known to inhibit N_2 fixation in photosynthetic bacteria. It also
350 effectively prevents photoproduction of H_2, due to inhibition and inactivation of nitrogenase (18).
351 The presence of ammonium in non-limiting amounts in the medium indicated that potentially H_2
352 production was driven by the hydrogenase rather than by the nitrogenase. The molar C:N ratio (5.7)
353 was 7 times lower than in most other studies on H_2 production (average C:N ratio 40) (58).
354 Nonetheless, the H_2 production rate per gram biomass during the 8 h light phases was around 11
355 times higher than in all other conditions (0.156 *vs* 0.014 mmol h^{-1} g^{-1} DW), indicating that H_2
356 production acts as further electron dissipation pathway. A similar H_2 production pattern under
357 alternate irradiation in PNSB cultures has been found (59), with H_2 production only during the light
358 phases. H_2 production was not integrated in the numerical model, since H_2 did not contribute

359 significantly to the stoichiometric balance and kinetics.

360

361 The absence of relevant H_2 production over 16 h light (0.004 ± 0.0004 mmol h^{-1}) and its low but
362 constant production during 8 h light (0.025 ± 0.009 mmol h^{-1}) indicates that the H_2 sink did not play
363 a major role in the electron redistribution patterns.

364

365 Overall, PNSB are one of the most versatile guilds of microorganisms. They present consistent
366 differences in their metabolisms, interspecies and intraspecies. We presented a comprehensive
367 explanation of the underlying mechanisms of electron allocation using quantitative biotechnology
368 and metabolic modelling. The numerical model represented well the biomass and nutrient dynamics
369 during the light/dark cycles of different durations. It allowed for determining stoichiometric and
370 kinetic parameters of the *Rhodopseudomonas*. It can be concluded that:

371 1) Under light-saturating conditions and continuous-flow reactor regime, durations of light and
372 dark phases in a diel cycle set the availability of substrate and the achievement of a steady
373 state. Longer dark phases result in an excess of substrate available in the light phase for
374 biomass growth. Longer light phases lead to substrate limitation and steady conditions.
375 2) Even in actively growing cells, carbon allocation is in place, namely toward PHA
376 production.
377 3) In growing cells, H_2 production during illumination is a minor electron sink and secondary
378 to PHA production.

379

Material and Methods

Strain

The *Rhodopseudomonas* strain was isolated with dilution series in agar from an in-house PNSB enrichment culture designed for nutrient removal from synthetic wastewater (30). The isolate was characterized by full-length 16S rRNA gene sequencing. The genomic DNA was extracted using UltraClean® Microbial DNA Isolation Kit (MO BIO Laboratories, Inc., USA), following manufacturer's instructions. The full 16S rRNA gene was amplified with the primers forward U515 (5'-GTGYCAGCMGCCGCGGTA-3') and reverse U1071 (5'-GARCTGRCGRCRRCCATGCA-3') (31), and sequenced for phylogenetic identification using a Sanger sequencing (Baseclear, NL). The sequence was aligned over the Blast database (32), and resulted in a 97.2% identity with *Rhodopseudomonas palustris*.

Medium

The inflow medium was adapted from Cerruti et al. (30). It consisted of (per liter): 0.914 g $CH_3COONa{\cdot}3H_2O$ (13.5 C-mmol L^{-1} or 54 mmol electrons L^{-1} when expressed via degree of reduction and 432 mg COD L^{-1} when expressed as chemical oxygen demand), 0.229 g NH_4Cl (*i.e.*, 4.281 mmol N L^{-1} or 60 mg N-NH_4^+ L^{-1}), 0.014 g KH_2PO_4 and 0.021 g K_2HPO_4 (*i.e.*, 0.223 mmol P L^{-1} or 7 mg P L^{-1}), 0.200 g $MgSO_4{\cdot}7H_2O$, 0.200 g NaCl, 0.050 g $CaCl_2{\cdot}2H_2O$, 1 mL vitamins solution, 1 mL trace element solution, and 4.7 g 4-(2-hydroxyethyl)-1-piperazineethanesulfonic acid (HEPES) used as pH buffer.

The vitamin solution was composed of (per liter): 200 mg thiamine–HCl, 500 mg niacin, 300 mg ρ-amino-benzoic acid, 100 mg pyridoxine–HCl, 50 mg biotin and 50 mg vitamin B12.

403 The trace element solution was composed of (per liter): 1100 mg Na EDTA·2H_2O, 2000 mg
404 $FeCl_3$·6H2O, 100 mg $ZnCl_2$, 64 mg $MnSO_4$·H_2O, 100 mg H_3BO_3, 100 mg $CoCl_2$·6H_2O, 24 mg
405 Na_2MoO_4·2H_2O, 16 mg $CuSO_4$·5H_2O, 10 mg $NiCl_2$·6H_2O and 5 mg $NaSeO_3$.
406
407 The medium components were sterilized though autoclavation or filtration with 0.22 μm filters
408 (Whatman, USA) (acetate solution, trace elements and vitamins).
409
410 **Reactor setup**
411 Continuous cultures were run to evaluate the influence of diel cycles on the physiology of PNSB. A
412 1.5-L continuous-flow stirred-tank reactor with 1.2-L working volume was connected to a
413 programmable logic controller (In-Control and Power unit, Applikon, NL) and operated under
414 stirring of 350 rpm, pH 7.0 ± 0.5, temperature of 30±1 °C during illumination phases and 20°C
415 during dark phases. Argon gas (Linde, NL, >99% purity) was sparged continuously in the bulk
416 liquid phase at 120 mL min^{-1} to maintain anaerobic conditions. The continuous-flow rate was set at
417 0.048 L h^{-1}. It corresponded to a dilution rate of 0.04 h^{-1} chosen based on the growth rate of the
418 strain previously measured at 0.11 h^{-1} (data not shown). The biomass was maintained at a low
419 concentration of 0.26 ± 0.05 g DW L^{-1} to minimize light shading effects.
420
421 The reactor was placed in a shaded hood to tightly control the irradiation patterns. Two halogen
422 floodlight lamps (Handson, NL) were positioned at opposite sides of the reactor diameter. The
423 incident white light spectrum was filtered for infrared (IR) light ($\lambda > 700$ nm) using two filter sheets
424 of 70 x 70 cm (Black Perspex 962, Plasticstockist, UK). The IR light intensity measured at the
425 reactor surface with a pyranometer (CMP3; Kipp & Zonen, NL) was 300 W m^{-2}. An automatic
426 device was used to switch on/off the light at required time sets. Three light conditions were tested:
427 1) continuous illumination (*i.e.*, 24 h light), 2) 16 h light and 8 h dark cycles, and 3) 8 h light and 16
428 h dark cycles.

Analytical methods

The biomass concentration was measured by absorbance at 660 nm (A_{660}) using a spectrophotometer (Biochrom, Libra S11, USA). A calibration curve was established to correlate A_{660} to dry weight (DW) concentration: c(g DW L^{-1}) = 0.64 A_{660} – 0.06. Biomass dry weight was measured taking samples from the liquid phase, filtering them using 0.45 µm filters (Whatman, USA) and storing them in a 70 °C stove for 72 h (adapted from Lip et al. 2020).

Acetate was measured with a high-performance liquid chromatograph (HPLC) (Waters, 2707, NL) equipped with an Aminex HPX-87H column (BioRad, USA). Samples were eluted using H_3PO_4 (1.5 mmol L^{-1}, flowrate of 0.6 mL min^{-1}, temperature of 60°C) prior to refraction index (Waters 2414) and UV (210 nm, Waters 484) detections.

Ammonium (as N-NH_4^+) and orthophosphate (as P-PO_4^{3-}) concentrations were measured with a discrete analyser (Thermoscientific Gallery, NL).

PHA measurements were performed with fluorimetry for high sensitivity on small biomass samples. The low biomass concentration did not allow for traditional extractions of PHA and gas chromatographic measurements of monomers. PHAs were stained in the biological samples with Nile red (CAS n. 7385-67-3, Sigma Aldricht), as in (34). Fluorescence was measured with a microplate reader (1000M pro, Tecan), with excitation at 535 nm and emission at 605 nm. The fluorescent counts were normalized by the g DW of biomass present in analysed samples. The absorbance at 660 nm was measured in each well, and then converted in gDW biomass, to this end.

453 The CO_2 and H_2 in the offgas were measured using a mass spectrometer (Thermofisher, Prima BT
454 Benchtop MS) connected online to the bioreactor. The production rates of these components were
455 calculated using the argon gas inflow rate (120 mL h^{-1}).
456
457 **Mathematical model**
458 A simple mathematical model was developed to characterize the behavior of the continuous culture
459 of *Rhodopseudomonas* exposed to light/dark cycles. Under light, photoorganoheterotrophic growth
460 was assumed; under dark, completely ceased metabolic activity. The growth stoichiometry with
461 light as energy source followed equation (1), with the biomass composition adapted from (35):

462 $$\frac{1}{Y_{XS}}\ CH_3COOH\ +\ Y_{NX}\ NH_4^+\ +\ Y_{PX}\ PO_4^{3-}\ +\ \lambda_{light} \rightarrow CH_{1.8}O_{0.38}N_{0.18}P_{0.014}\ +\ Y_{CX}\ CO_2\ +\ Y_{WX}\ H_2O\ +\ Y_{HX}\ H^+ \quad (1)$$

463
464 The process was described by a system of balance equations for the relevant materials in the mixed
465 liquor (eqns. (2) (biomass C_X , acetic acid C_S, ammonium C_N, phosphate C_P and carbon dioxide C_C).

466 $$\frac{dC_X}{dt} = \frac{F}{V}\cdot\left(-C_X\right) + r_X\,, \qquad \frac{dC_C}{dt} = \frac{F}{V}\cdot\left(-C_C\right) + r_C + k_L a\cdot\left(C_C^* - C_C\right) \quad (2)$$

467 $$\frac{dC_S}{dt} = \frac{F}{V}\cdot\left(C_{S,in} - C_S\right) + r_S\,,\ \frac{dC_N}{dt} = \frac{F}{V}\cdot\left(C_{N,in} - C_N\right) + r_N\,,\quad \frac{dC_P}{dt} = \frac{F}{V}\cdot\left(C_{P,in} - C_P\right) + r_P$$

468
469 A gas phase balance was integrated for the CO_2 concentration in the gas $C_{C,g}$ (mmol/L):

470 $$\frac{dC_{C,g}}{dt} = -\frac{F_g}{V_g}C_{C,g} - k_L a\cdot\left(C_C^* - C_C\right)\cdot\frac{V}{V_g} \quad (3)$$

471
472 The volumetric growth rate, r_X (C-mmol X L^{-1} h^{-1}), was assumed to be limited by the
473 concentrations of multiple chemical compounds and by light intensity I (W m^{-2}):

$$r_X = \mu_{max} \cdot \frac{C_S}{K_S + C_S} \cdot \frac{C_N}{K_N + C_N} \cdot \frac{C_P}{K_P + C_P} \cdot \frac{I}{K_I + I} \cdot C_X \quad (4)$$

The uptake and production rates of chemical compounds (mmol L^{-1} h^{-1}) follow from the reaction stoichiometry and biomass growth rate:

$$r_S = -\frac{1}{Y_{XS}} \cdot r_X, \qquad r_N = -Y_{NX} \cdot r_X, \qquad r_P = -Y_{PX} \cdot r_X, \qquad r_{CO2} = Y_{CX} \cdot r_X$$

Similarly, the biomass-specific rates were calculated as $q_S = \mu / Y_{XS}$, $q_N = Y_{NX}\mu$, $q_P = Y_{PX}\mu$ and $q_C = Y_{CX}\mu$. The yields Y_{XS}, Y_{CX} and max. specific growth rate μ_{max} were determined by fitting the measurements from the 16h light / 8h dark experiment with this model. Additional estimations of the μ_{max} based on batches and chemostat experiments under continuous illumination and light / dark patterns resulted in μ_{max} values of 0.14 ±0.05. The yields Y_{NX} and Y_{PX} (and consequently the N and P biomass composition *nN* and *nP*, respectively) were determined from the 8h light / 16h dark experiment, for which we were able to record better quality data.

The liquid flow rate F (L h^{-1}) and volume V (L), the gas flow rate F_g (L h^{-1}) and volume V_g (L), as well as the concentrations of chemical compounds in the influent C_{in} (mmol L^{-1}) were all fixed in the experiments. The volumetric mass transfer coefficient k_La (h^{-1}) was determined from the correlation with the power input, liquid volume, and gas velocity (see SI-1). The dissolved CO_2 concentration, C_C^* (mmol L^{-1}), was calculated function of gas concentration $C_{C,g}$, Henry coefficient H_C (mol L^{-1} atm^{-1}) and respective temperature (20°C in dark and 30°C in light) and pressure (1 atm).

Two light sources with intensity I_0 were placed at opposite sides next to the reactor. The light intensity decrease away from the reactor wall was assumed to follow the Beer-Lambert attenuation

497 law. Therefore, by summing the light intensities coming from both sides one obtains the total light
498 intensity I_t at a radial position x (m) in the reactor:

499 $$I_t = I_0 \cdot \left(e^{-\varepsilon \cdot c_X \cdot x} + e^{-\varepsilon \cdot c_X \cdot (2 \cdot R - x)} \right) \quad (5)$$

500 with R (m) the reactor radius, ε (m^2 g^{-1}) the biomass-specific light attenuation coefficient and C_X
501 (g m^{-3}) the biomass concentration. We considered that due to liquid mixing the cells will be exposed
502 to an average light intensity I (W m^{-2}) computed by integrating eq. (5) over the reactor diameter:

503 $$I = I_0 \cdot \frac{1 - e^{-2 \cdot \varepsilon \cdot c_X \cdot R}}{\varepsilon \cdot c_X \cdot R} \quad (6)$$

504 The model was solved in MATLAB (R2018b, Mathworks, Natick, MA, www.mathworks.com)
505 using a stiff solver for the ordinary differential equations system (2) and (3). The initial
506 concentrations where taken to coincide with the measurements. The parameter estimation was
507 performed by a constrained optimization routine minimizing the sum of squares of relative errors
508 between model and experimental data. The fixed model parameters and the fitted parameters are
509 listed in Table 1. A more extensive description of the parameter used is available in SI-1.
510

Acknowledgements

This study was financed by the tenure-track start-up grant of the Department of Biotechnology of the Faculty of Applied Sciences of the TU Delft (David Weissbrodt, PI). We acknowledge the Onassis Foundation for the financial support in the scholarship of Viktor Chasna. We also thank Dirk Geerts and Rob Kerste for technical assistance with the reactor infrastructure and fermentation facility, Katie Thorp for the isolation of the culture and Gijs Kuenen for the valuable discussions.

Conflict of interest statement

The authors declare no conflict of interest.

Preprint

This manuscript will be deposited as pre-print in bioRxiv.

Supplementary information

Appendix 1: Estimation of the kLa of the process

Appendixes 2: Mathematical model simulations

- Fig. A-1: Data and simulation of the 8 h light / 16 h dark cycles with extended light phase.
- Fig. A-2: Model results for the light intensity inside the reactor
- Fig. A-3: Model results for production and uptake rate in the 16 h light / 8 h dark cycles
- Fig. A-4: Model results for production and uptake rate in the 8 h light / 16 h dark cycles.

References

1. Blankenship R, Madigan M, Bauer C. Anoxygenic Photosynthetic Bacteria. Blankenship RE, Madigan MT, Bauer CE, editors. Dordrecht: Springer Netherlands; 1995. 595–626 p. (Advances in Photosynthesis and Respiration; vol. 2).
2. Alloul A, Wuyts S, Lebeer S, Vlaeminck SE. Volatile fatty acids impacting phototrophic growth kinetics of purple bacteria: Paving the way for protein production on fermented wastewater. Water Res. 2019;152:138–47.
3. Madigan MT, Jung DO. An Overview of Purple Bacteria: Systematics, Physiology, and Habitats. In: Hunter CN, Daldal F, Thurnauer MC, Beatty JT, editors. The Purple Phototrophic Bacteria. Dordrecht: Springer Netherlands; 2009. p. 1–15.
4. Hülsen T, Hsieh K, Lu Y, Tait S, Batstone DJ. Simultaneous treatment and single cell protein production from agri-industrial wastewaters using purple phototrophic bacteria or microalgae – A comparison. Bioresour Technol. 2018;254:214–23.
5. Wang H, Yang A, Zhang G, Ma B, Meng F, Peng M, et al. Enhancement of carotenoid and bacteriochlorophyll by high salinity stress in photosynthetic bacteria. Int Biodeterior Biodegradation. 2017;121:91–6.
6. Vincenzini M, Marchini A, Ena A, De Philippis R. H2 and poly-β-hydroxybutyrate, two alternative chemicals from purple non sulfur bacteria. Biotechnol Lett. 1997;19(8):759–62.
7. Hustede E, Steinbüchel A, Schlegel HG. Relationship between the photoproduction of hydrogen and the accumulation of PHB in non-sulphur purple bacteria. Appl Microbiol Biotechnol. 1993;39(1):87–93.
8. Madigan M, Cox JC, Gest H. Photopigments in *Rhodopseudomonas capsulata* cells grown anaerobically in darkness. J Bacteriol. 1982;150(3):1422–9.
9. Imhoff JF. Taxonomy and Physiology of Phototrophic Purple Bacteria and Green Sulfur Bacteria. In: Blankenship RE, Madigan MT, Bauer CE, editors. Anoxygenic Photosynthetic

Bacteria. Dordrecht: Springer Netherlands; 1995. p. 1–15.

10. Madigan MT, Bender K, Buckley D, Sattley M, Stahl D. Brock Biology of Microorganisms. Fourtheen Edition. Vol. 1, Pearson. Pearson; 2015. 1–1041 p.

11. Green J, Paget MS. Bacterial redox sensors. Nat Rev Microbiol. 2004;2(12):954-66.

12. Laguna R, Tabita FR, Alber BE. Acetate-dependent photoheterotrophic growth and the differential requirement for the Calvin-Benson-Bassham reductive pentose phosphate cycle in *Rhodobacter sphaeroides* and *Rhodopseudomonas palustris*. Arch Microbiol. 2011;193(2):151–4.

13. Dupuis A, Chevallet M, Darrouzet E, Duborjal H, Lunardi J, Issartel JP. The Complex I from *Rhodobacter capsulatus*. Biochim Biophys Acta - Bioenerg. 1998;1364(2):147–65.

14. Spero AM, Saheed I, Noguera DR, Donohue TJ. Cytochrome Complexes: Evolution, Structures, Energy Transduction, and Signaling. 2016;41:237–51.

15. McKinlay JB, Harwood CS. Calvin cycle flux, pathway constraints, and substrate oxidation state together determine the H_2 biofuel yield in photoheterotrophic bacteria. MBio. 2011;2(2):e00323-10.

16. Gordon GC, McKinlay JB. Calvin cycle mutants of photoheterotrophic purple nonsulfur bacteria fail to grow due to an electron imbalance rather than toxic metabolite accumulation. J Bacteriol. 2014;196(6):1231-1237.

17. Kim JS, Ito K, Takahashi H. The Relationship between Nitrogenase Activity and Hydrogen Evolution in *Rhodopseudomonas palustris*. Agric Biol Chem. 1980;44(4):827–33.

18. Basak N, Jana AK, Das D, Saikia D. Photofermentative molecular biohydrogen production by purple-non-sulfur (PNS) bacteria in various modes: The present progress and future perspective. Vol. 39, International Journal of Hydrogen Energy. 2014. p. 6853–71.

19. Oda Y, Samanta SK, Federico †, Rey E, Wu L, Liu X, et al. Functional Genomic Analysis of Three Nitrogenase Isozymes in the Photosynthetic Bacterium *Rhodopseudomonas palustris*. J Bacteriol. 2005;187(22):7784–94.

20. McKinlay JB, Oda Y, Ruhl M, Posto AL, Sauer U, Harwood CS. Non-growing *Rhodopseudomonas palustris* increases the hydrogen gas yield from acetate by shifting from the glyoxylate shunt to the tricarboxylic acid cycle. J Biol Chem. 2014;

21. Willison JC, Jouanneau Y, Colbeau A, Vignais PM. H2 metabolism in photosynthetic bacteria and relationship to N_2 fixation. Ann l'Institut Pasteur / Microbiol. 1983 Jul;134(1):115–35.

22. Kutralam-Muniasamy G, Corona-Hernandez J, Narayanasamy RK, Marsch R, Pérez-Guevara F. Phylogenetic diversification and developmental implications of poly-(R)-3-hydroxyalkanoate gene cluster assembly in prokaryotes. FEMS Microbiol Lett. 2017;364(13):1–9.

23. Montano-Herrera L, Laycock B, Werker A, Pratt S. The evolution of polymer composition during PHA accumulation: The significance of reducing equivalents. Bioengineering. 2017;4(1):20.

24. Hustede E, Steinbiichel A, Schlegel HG. Cloning of poly(3-hydroxybutyric acid) synthase genes of *Rhodobacter sphaeroides* and *Rhodospirillum rubrum* and heterologous expression in *Alcaligenes eutrophus*. FEMS Microbiol Lett. 1992;93:285–91.

25. Haywood GW, Anderson AJ, Chu L, Dawes EA. The role of NADH- and NADPH-linked acetoacetyl-CoA reductases in the poly-3-hydroxybutyrate synthesizing organism *Alcaligenes eutrophus*. FEMS Microbiol Lett. 1988;52(3):259–64.

26. De Philippis R, Ena A, Guastiini M, Sili C, Vincenzini M. Factors affecting poly-β-hydroxybutyrate accumulation in cyanobacteria and in purple non-sulfur bacteria. FEMS Microbiol Lett. 1992;103(2–4):187–94.

27. Higuchi-Takeuchi M, Morisaki K, Toyooka K, Numata K. Synthesis of high-molecular-weight polyhydroxyalkanoates by marine photosynthetic purple bacteria. PLoS One. 2016;11(8): e0160981.

28. Bardone E, Bravi M, Keshavarz T, Padovani G, Carlozzi P, Seggiani M, et al. PHB-Rich

Biomass and BioH 2 Production by Means of Photosynthetic Microorganisms. Chem Eng Trans. 2016;49.

29. Hustede E, Steinbüchel A, Schlegel HG. Relationship between the photoproduction of hydrogen and the accumulation of PHB in non-sulphur purple bacteria. Appl Microbiol Biotechnol. 1993;39:87–93.

30. Cerruti M, Stevens B, Ebrahimi S, Alloul A, Vlaeminck SE, Weissbrodt DG. Enriching and aggregating purple non-sulfur bacteria in an anaerobic sequencing-batch photobioreactor for nutrient capture from wastewater. bioRxiv 2020;2020.01.08.899062.

31. Wang Y, Qian P-Y. Conservative Fragments in Bacterial 16S rRNA Genes and Primer Design for 16S Ribosomal DNA Amplicons in Metagenomic Studies. PLoS One. 2009;4(10):7401.

32. Altschul SF, Gish W, Miller W, Myers EW, Lipman DJ. Basic local alignment search tool. J Mol Biol. 1990;215(3):403–10.

33. Lip KYF, García-Ríos E, Costa CE, Guillamón JM, Domingues L, Teixeira J, et al. Selection and subsequent physiological characterisation of industrial *Saccharomyces cerevisiae* strains during continuous growth at sub- and- supra optimal temperatures. bioRxiv. 2020;2020.01.30.926709

34. Zuriani R, Vigneswari S, Azizan MNM, Majid MIA, Amirul AA. A high throughput Nile red fluorescence method for rapid quantification of intracellular bacterial polyhydroxyalkanoates. Biotechnol Bioprocess Eng. 2013;18(3):472–8.

35. McKinlay JB, Harwood CS. Carbon dioxide fixation as a central redox cofactor recycling mechanism in bacteria. Proc Natl Acad Sci. 2010;107(26):11669–75.

36. Kaewsuk J, Thorasampan W, Thanuttamavong M, Seo GT. Kinetic development and evaluation of membrane sequencing batch reactor (MSBR) with mixed cultures photosynthetic bacteria for dairy wastewater treatment. J Environ Manage. 2010;91(5):1161–8.

635 37. Wolf G, Picioreanu C, van Loosdrecht MCM. Kinetic Modeling of Phototrophic Biofilms:
636 The PHOBIA Model. Biotechnol Bioeng. 2007;97:1064–79.
637 38. Puyol D, Barry EM, Hülsen T, Batstone DJ. A mechanistic model for anaerobic phototrophs
638 in domestic wastewater applications: Photo-anaerobic model (PAnM). Water Res. 2017;116:
639 241-253.
640 39. Prachanurak P, Chiemchaisri C, Chiemchaisri W, Yamamoto K. Modelling of biofilm
641 growth for photosynthetic biomass production in a pipe-overflow recirculation bioreactor.
642 Biochem Eng J. 2019;142:50–7.
643 40. Sander R. Compilation of Henry's law constants (version 4.0) for water as solvent. Atmos
644 Chem Phys. 2015;15(8):4399–981.
645 41. Oehmen A, Zeng RJ, Saunders AM, Blackall LL, Keller J, Yuan Z. Anaerobic and aerobic
646 metabolism of glycogen-accumulating organisms selected with propionate as the sole carbon
647 source. Microbiology. 2006;152(9):2767–78.
648 42. Montiel Corona V, Le Borgne S, Revah S, Morales M. Effect of light-dark cycles on
649 hydrogen and poly-β-hydroxybutyrate production by a photoheterotrophic culture and
650 Rhodobacter capsulatus using a dark fermentation effluent as substrate. Bioresour Technol.
651 2017;226:238–46.
652 43. Zhi R, Yang A, Zhang G, Zhu Y, Meng F, Li X. Effects of light-dark cycles on
653 photosynthetic bacteria wastewater treatment and valuable substances production. Bioresour
654 Technol. 2019;274:496–501.
655 44. Koku H, Eroglu I, Gündüz U, Yücel M, Türker L. Kinetics of biological hydrogen
656 production by the photosynthetic bacterium *Rhodobacter sphaeroides* O.U. 001. Int J
657 Hydrogen Energy. 2003;28(4):381–8.
658 45. Li X, Wang Y, Zhang S, Chu J, Zhang M, Huang M, et al. Effects of light/dark cycle, mixing
659 pattern and partial pressure of H2 on biohydrogen production by *Rhodobacter sphaeroides*
660 ZX-5. Bioresour Technol. 2011;102(2):1142–8.

661 46. Wakayama T, Nakada E, Asada Y, Miyake J. Effect of light/dark cycle on bacterial hydrogen
662 production by *Rhodobacter sphaeroides* RV: From hour to second range. Appl Biochem
663 Biotechnol - Part A Enzym Eng Biotechnol. 2000;84–86:431–40.
664 47. Brotosudarmo THP, Collins AM, Gall A, Roszak AW, Gardiner AT, Blankenship RE, et al.
665 The light intensity under which cells are grown controls the type of peripheral light-
666 harvesting complexes that are assembled in a purple photosynthetic bacterium. Biochem J.
667 2011;440(1):51–61.
668 48. Imam S, Fitzgerald CM, Cook EM, Donohue TJ, Noguera DR. Quantifying the effects of
669 light intensity on bioproduction and maintenance energy during photosynthetic growth of
670 *Rhodobacter sphaeroides*. Photosynth Res. 2015;123(2):167–82.
671 49. Van Aalst-Van Leeuwen MA, Pot MA, Van Loosdrecht MCM, Heijnen JJ. Kinetic modeling
672 of poly(β-hydroxybutyrate) production and consumption by *Paracoccus pantotrophus* under
673 dynamic substrate supply. Biotechnol Bioeng. 1997;55(5):773–82.
674 50. van Loosdrecht MCM, Pot MA, Heijnen JJ. Importance of bacterial storage polymers in
675 bioprocesses. Water Sci Technol. 1997;35(1):41–7.
676 51. Narancic T, Scollica E, Kenny ST, Gibbons H, Carr E, Brennan L, et al. Understanding the
677 physiological roles of polyhydroxybutyrate (PHB) in *Rhodospirillum rubrum* S1 under
678 aerobic chemoheterotrophic conditions. Appl Microbiol Biotechnol. 2016;100(20):8901–12.
679 52. Braunegg G, Lefebvre G, Genser KF. Polyhydroxyalkanoates, biopolyesters from renewable
680 resources: Physiological and engineering aspects. J Biotechnol. 1998;65(2–3):127–61.
681 53. McKinlay JB, Oda Y, Ruhl M, Posto AL, Sauer U, Harwood CS. Non-growing
682 *Rhodopseudomonas palustris* increases the hydrogen gas yield from acetate by shifting from
683 the glyoxylate shunt to the tricarboxylic acid cycle. J Biol Chem. 2014 Jan 24;289(4):1960–
684 70.
685 54. Satoh Y, Tajima K, Tannai H, Munekata M. Enzyme-catalyzed poly(3-hydroxybutyrate)
686 synthesis from acetate with CoA recycling and NADPH regeneration in vitro. J Biosci

687 Bioeng. 2003;95(4):335–41.

688 55. Kanno N, Matsuura K, Haruta S. Different Metabolomic Responses to Carbon Starvation
689 between Light and Dark Conditions in the Purple Photosynthetic Bacterium,
690 *Rhodopseudomonas palustris*; Microbes Environ. 2018;33(1):83–8.

691 56. Kranz RG, Gabbert KK, Locke TA, Madigan MT. Polyhydroxyalkanoate production in
692 *Rhodobacter capsulatus*: Genes, mutants, expression, and physiology. Appl Environ
693 Microbiol. 1997;63(8):3003–9.

694 57. Krishna C, Van Loosdrecht MCM. Effect of temperature on storage polymers and
695 settleability of activated sludge. Water Res. 1999;33(10):2374–82.

696 58. Koku H, Eroglu I, Gündüz U, Yücel M, Türker L. Aspects of the metabolism of hydrogen
697 production by *Rhodobacter sphaeroides*. Int J Hydrogen Energy. 2002;27(11–12):1315–29.

698 59. Adessi A, Torzillo G, Baccetti E, De Philippis R. Sustained outdoor H_2 production with
699 *Rhodopseudomonas palustris* cultures in a 50 L tubular photobioreactor. Int J Hydrogen
700 Energy. 2012;37:8840–9.

701 60. van't Riet K, Tramper J. Basic Bioreactor Design. CRC Press; 1991.

702 61. Liu K, Phillips JR, Sun X, Mohammad S, Huhnke RL, Atiyeh HK. Investigation and
703 Modeling of Gas-Liquid Mass Transfer in a Sparged and Non-Sparged Continuous Stirred
704 Tank Reactor with Potential Application in Syngas Fermentation. Fermentation.
705 2019;5(3):75.

706 62. Okubo A. Diffusion: Mass Transfer in Fluid Systems. E. L. Cussler . Q Rev Biol.
707 1987;62(1):131–131.

708

Figure legends

Figure 1. Schematic representation of the reducing power allocation in *Rhodopseudomonas*. Red lines: electron flow; Black dashed lines: proton transfer; Blue dotted lines: NADH is normally produced in the catabolic processes, whereas NADPH is used in the anabolic processes, such as PHAs formation. Biomass and CBB are the primary electron sinks in PNSB. PHAs and H_2 are two of the other possible electron sinks.

Figure 2. Dynamics of biomass, acetate, ammonium and phosphate concentrations during light-dark cycles: (A),(C) 16 h light / 8 h dark; (B),(D) 8 h light / 16 h dark. Gray areas represent the dark periods. (A),(B) biomass (black circles) and acetate (red open squares) measured concentrations, with lines being the model results. The biomass concentration achieved a stationary state, while acetate reached very low (limiting) concentrations after 2 h of the 16 h light periods. The biomass increased without reaching a steady state during the 8 h light periods, while acetate was not fully consumed. (C),(D) ammonium (blue diamonds) and phosphate (green triangles) measured concentrations, with lines being the model results. Concentrations of N and P were not limiting for the system in any illumination phase.

Figure 3. Dynamics of CO_2, H_2 and PHA during light-dark cycles: (A),(D) continuous illumination; (B),(E),(G) 16 h light / 8 h dark; (C),(F),(H) 8 h light / 16 h dark. Gray areas represent the dark periods. (A),(B),(C) CO_2 production rate - measured (red circles) and computed (lines). CO_2 production was constant during continuous illumination, but peaks appeared during light-dark cycles, correlated with the acetate uptake. (D),(E),(F) measured H_2 production (blue circles). Constant low level H_2 was produced during continuous illumination and 16 h light cycles, but H_2 production strongly increased in each light period of the 8 h light cycles. (G),(H) PHAs fluorescent counts per gram biomass in the light/dark experiments. A PHAs peak was measured at the beginning of each light phase under the 16 h light conditions, however less clear pattern could be detected under the 8 h light experiments.

734 # Tables

735 **Table 1.** Model parameters. The maximum biomass-specific growth rate and yields were fitted to experimental data,
736 while the other parameters were measured during experiments, calculated or obtained from literature.

Parameter name	Symbol	Value	Units	Source
Max. biomass-specific growth rate	μ_{max}	0.15	C-mol X · h^{-1} · C-mol^{-1} X	Fitted
Biomass yield	Y_{XS}	0.88	C-mol X · C-mol-1 S	Fitted
Ammonium yield	Y_{NX}	0.18	mol · C-mol^{-1} X	Fitted
Phosphate yield	Y_{PX}	0.009	mol · C-mol^{-1} X	Fitted
CO_2 yield	Y_{CX}	0.142	mol · C-mol^{-1} X	Fitted
Reactor radius	R	0.055	m	Measured
Liquid volume	V	1.2	L	Measured
Liquid flow rate	F	0.048	L·h^{-1}	Measured
Dilution rate	D	0.04	h^{-1}	F/V
Gas volume	V_g	0.3	L	Measured
Gas flow rate	F_g	7.14	L·h^{-1}	Measured
Inflow acetate concentration	$C_{S,in}$	7	mM	Measured
Inflow ammonium concentration	$C_{N,in}$	4.28	mM	Measured
Inflow phosphate concentration	$C_{P,in}$	0.22	mM	Measured
Light intensity at reactor walls	I_0	300	W·m^{-2}	Measured
Light extinction coefficient per biomass concentration	ε	0.1	m^2·g^{-1}	(17)
Half-saturation coefficient acetate	K_S	0.1	mM	Lower than in (36) (0.3 mM)
Half-saturation coefficient ammonium	K_N	0.001	mM	(37)
Half-saturation coefficient phosphate	K_P	0.003	mM	(38)
Half-saturation coefficient light	K_I	10	W·m^{-2}	(39)
CO_2 mass transfer coefficient	k_La	32	h^{-1}	Calculated (SI-1)
Henry coefficient CO_2	H_C	0.03 (at 30°C) 0.04 (at 20°C)	mol·L^{-1}·atm^{-1}	(40)

737

738

739 **Table 2.** Distribution of the carbon sources and carbon balances in different illumination conditions

Light/dark regimes	**Carbon inputs (C-mmol h^{-1})**	**Carbon outputs (C-mmol h^{-1})**				**Carbon balance (% C)**	**Electron balance (% COD)**
Component	Acetate	Acetate	Biomass	CO_2	Σ out		
Phase	Influent	Effluent	Effluent	Off-gas			
24 h light	0.66±0.05	<LOD[a]	0.58	0.07±0.001	0.65	98%	98%
16 h light	0.66±0.05	0.11±0.01	0.57±0.01	0.08±0.01	0.75±0.01	115±2%	113±1%
8 h dark		0.10±0.02	0.51±0.03	0.07±0.02	0.68±0.06	103±9%	102±9%
8 h light	0.61±0.006	0.28±0.03	0.62±0.05	0.07±0.01	0.97±0.05	158±8%[b]	159±9%[b]
16 h dark		0.19±0.07	0.57±0.12	0.03±0.002	0.79±0.15	130±25%[b]	137±27%[b]

740 [a] limit of detection; [b] the overvaluation of the carbon and electron balance can be due to an overestimation of the biomass concentration. The
741 absorbance measures taken might have influenced by the presence of PHAs inside the cells.

742

Supplementary information

Appendix 1: Estimation of the kLa's of the process

The overall mass transfer coefficients of the process were found in the CO_2 and O_2 mass balances. The calculation of the oxygen mass transfer coefficient was performed considering the equation for salt solutions

$$kLa\ (s^{-1}) = 0.002 \cdot \left(\frac{P}{V_{liquid}}\right)^{0.7} \cdot u_{gas}^{0.4}$$

where P is the power input (W), u_{gas} is the superficial gas velocity (m/s) and V_{liquid} the liquid volume (m^3). The power input was calculated through the following equation (60)

$$P(W) = \rho \cdot N_p \cdot N_i^3 D_i^5$$

where ρ is the density (kg m^{-3}) of the solution, N_p is the impeller power number, N_i is the impeller rotating speed (s^{-1}) and D_i is the impeller diameter(m).

The power number of the impeller is a function of the impeller type and the Reynolds number of the impeller. Reynolds was calculated through the following equation

$$Re = \frac{\rho N_i D_i^2}{\mu}$$

where μ is the viscosity of the solvent (Pa·s). Considering the density (997 kg m^{-3}) and viscosity of water in 25 ˚C (0.00089 Pa·s) the Reynolds impeller was slightly higher than 10^5. For that Reynolds and for a 6-blade Rushton turbine impeller the power number is around 5~6 (60). For the calculations, a power number of 6 was assumed. The diameter of the impeller was around 4 cm and the rotating speed 350 rpm (5.83 s^{-1}). Using those values the power input of the impeller was found equal to 0.101 W.

768 The superficial gas velocity was calculated by dividing the gas flowrate (7.14 L h^{-1}) with the surface
769 area (π R^2). The reactor radius R was 5.5 cm. After dividing and correcting for the units the
770 calculated superficial gas velocity was 0.000209 m s^{-1}. Using the calculated values of the superficial
771 gas velocity, power input and liquid volume ($1.2 \cdot 10^{-3}$ m^3) the k_La of oxygen was found equal to
772 33.52 (h^{-1}).
773 The k_La of carbon dioxide was found equal to 32 (h^{-1}) through the following equation (61). The
774 diffusion coefficient used are $1.92 \cdot 10^{-5}$ cm^2 s^{-1} (62)
775
776 $$kLa_x = \frac{kLa_{CO_2}}{\sqrt{\frac{D_{CO_2}}{D_x}}}$$
777

Appendixes 2 to 5: Mathematical model simulations

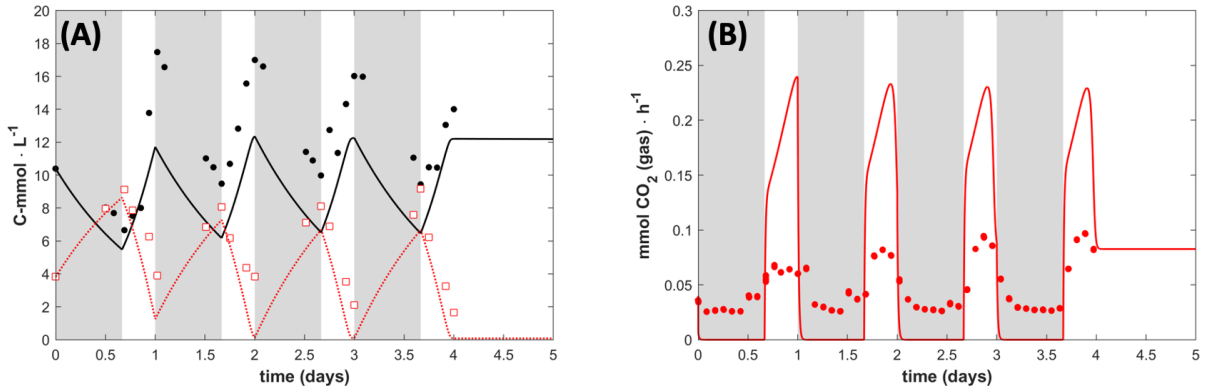

Figure A-2. Data and simulation with an additional extended light phase after the 8 h light 16 h dark cycles. (A) Biomass (black circles) and acetate (red open squares) measured concentrations, with lines being the model results. (B) Measured (red circles) and model prediction (line) of the CO_2 production rate A steady state is reached once the concentration of acetate is at its minimum.

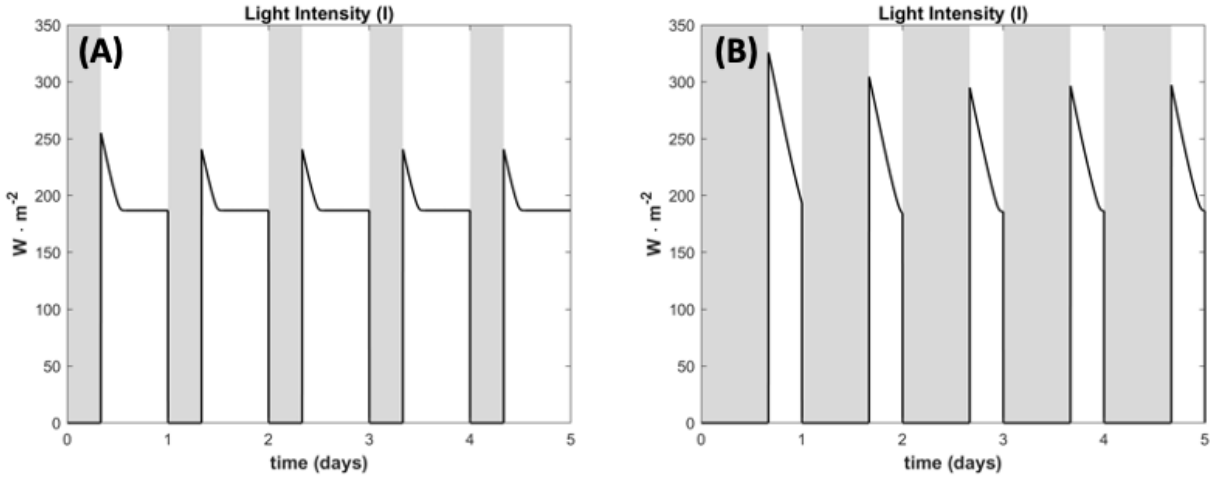

Figure A-3. Model results for the light intensity inside the reactor. (A) 16 h light / 8 h dark cycles. (B) 8 h light / 16 h dark cycles. Under any given condition light became a limiting factor.

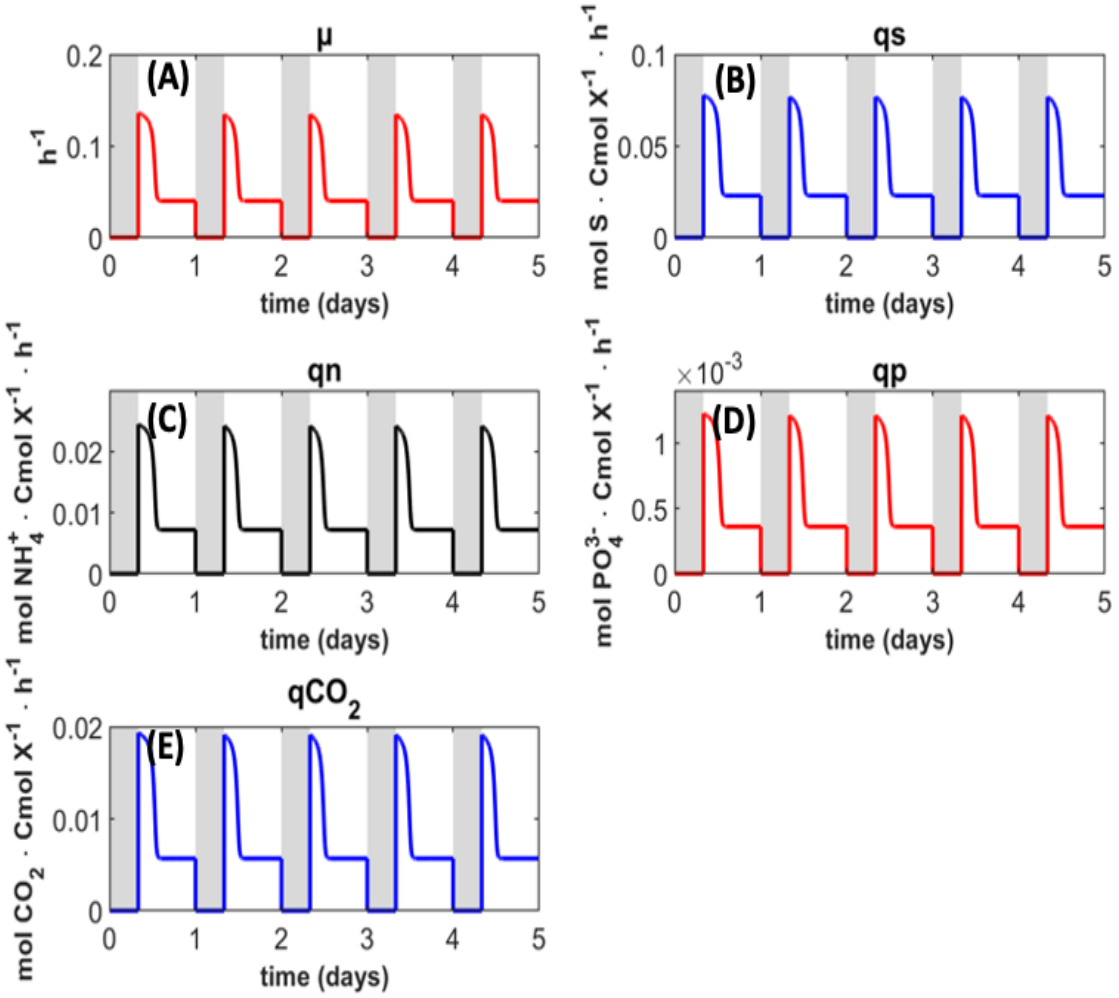

789

790 **Figure A-4.** Model results for production and uptake rate in the 16 h light / 8 h dark cycles. (A) specific growth rate. (B

791 specific acetate uptake rate. (C) specific ammonium uptake rate. (D) specific phosphate uptake rate. (E) specific CO_2

792 production rate.

793

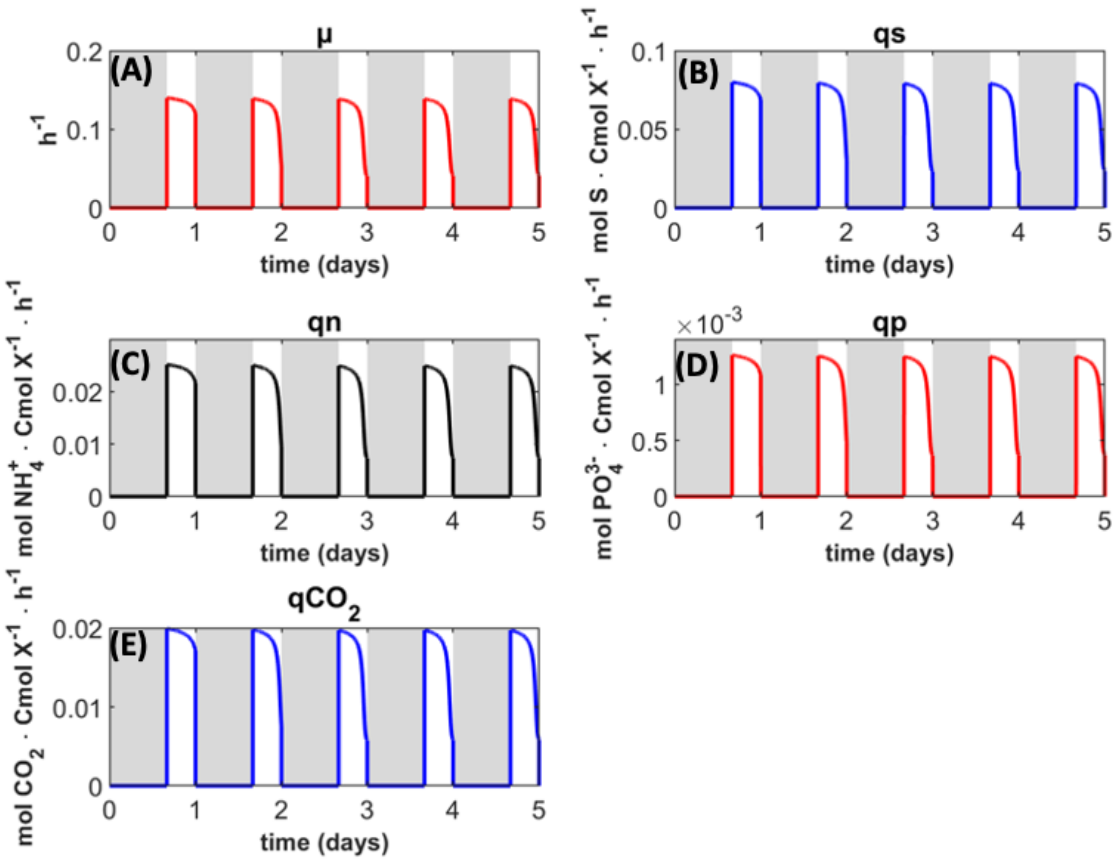

794

795 **Figure A-5.** Model results for production and uptake rate in the 8 h light / 16 h dark cycles. (A) specific growth rate. (B

796 specific acetate uptake rate. (C) specific ammonium uptake rate. (D) specific phosphate uptake rate. (E) specific CO_2

797 production rate.

798

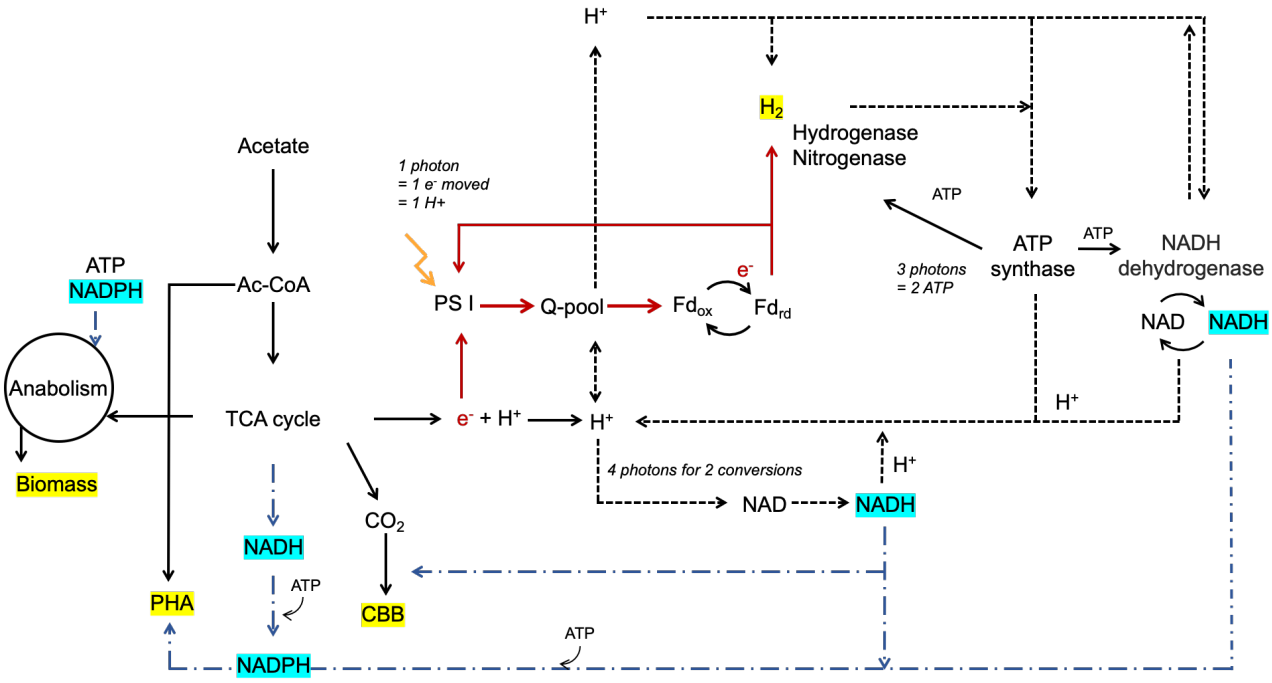

Figure 1. Schematic representation of the reducing power allocation in Rhodopseudomonas. Red lines: electron flow; Black dashed lines: proton transfer; Blue dotted lines: NADH is normally produced in the catabolic processes, whereas NADPH is used in the anabolic processes, such as PHAs formation. Biomass and CBB are the primary electron sinks in PNSB. PHAs and H_2 are two of the other possible electron sinks.

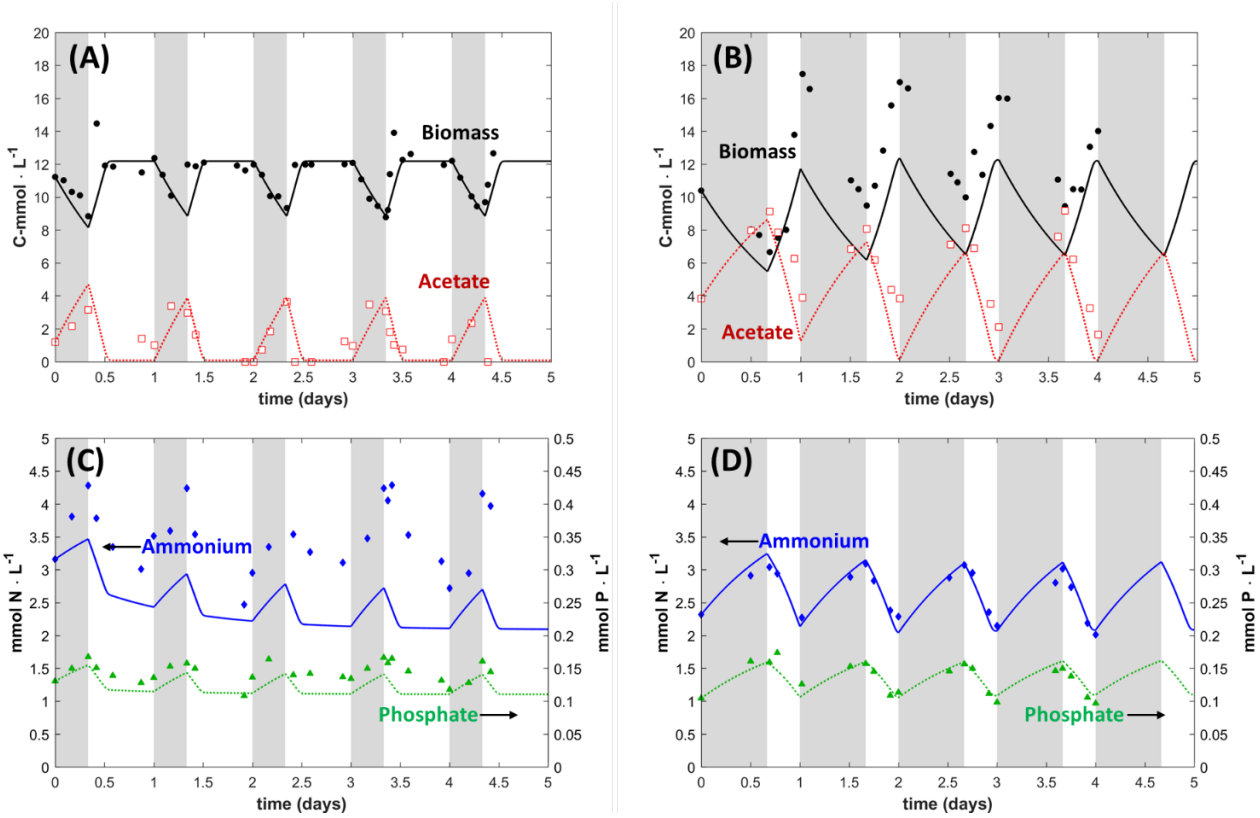

Figure 2. Dynamics of biomass, acetate, ammonium and phosphate concentrations during light-dark cycles: (A),(C) 16 h light / 8 h dark; (B),(D) 8 h light / 16 h dark. Gray areas represent the dark periods. (A),(B) biomass (black circles) and acetate (red open squares) measured concentrations, with lines being the model results. The biomass concentration achieved a stationary state, while acetate reached very low (limiting) concentrations after 2 h of the 16 h light periods. The biomass increased without reaching a steady state during the 8 h light periods, while acetate was not fully consumed. (C),(D) ammonium (blue diamonds) and phosphate (green triangles) measured concentrations, with lines being the model results. Concentrations of N and P were not limiting for the system in any illumination phase.

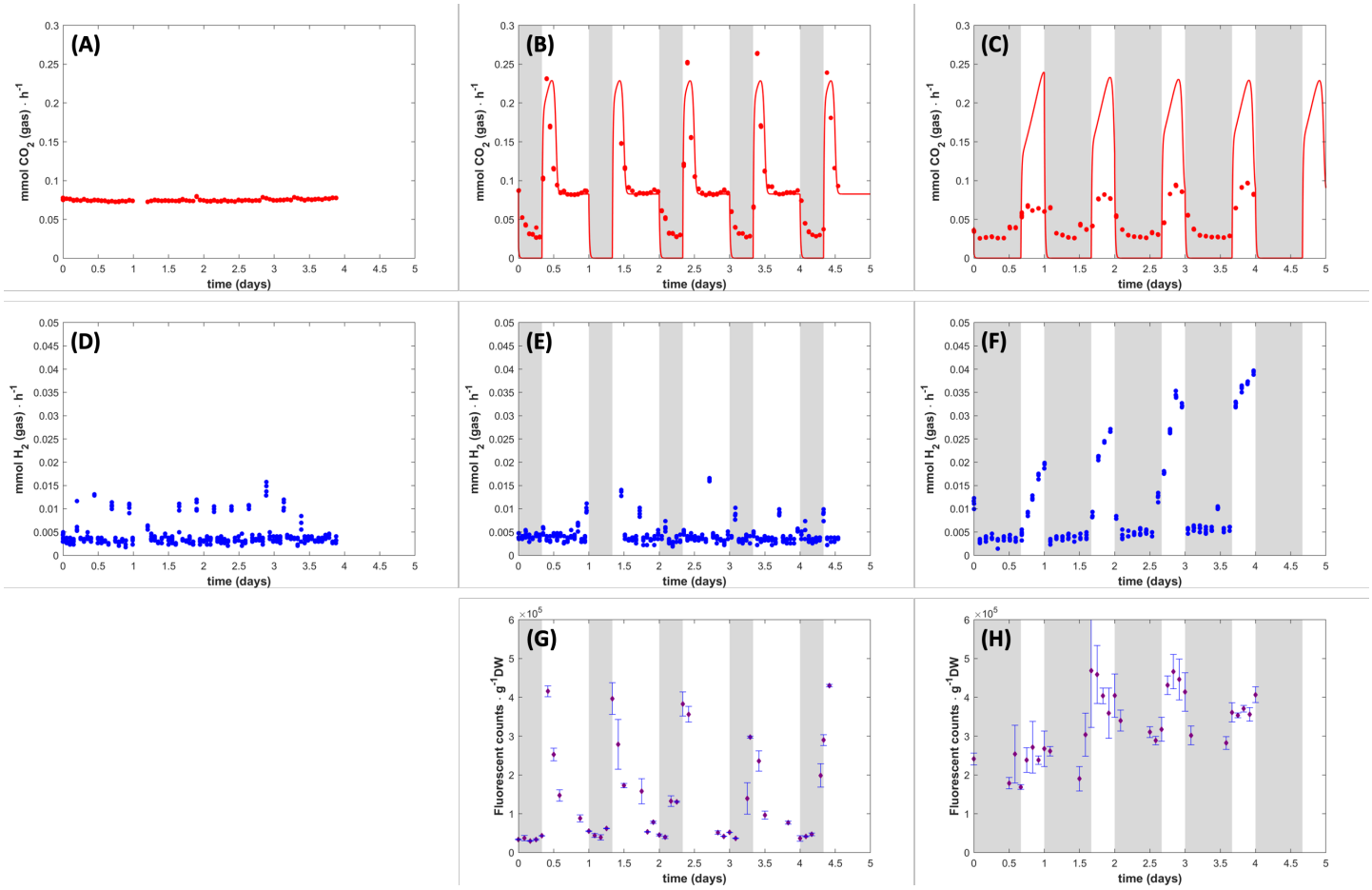

Figure 3. Dynamics of CO_2, H_2 and PHA during light-dark cycles: (A),(D) continuous illumination; (B),(E),(G) 16 h light / 8 h dark; (C),(F),(H) 8 h light / 16 h dark. Gray areas represent the dark periods. (A),(B),(C) CO_2 production rate - measured (red circles) and computed (lines). CO_2 production was constant during continuous illumination, but peaks appeared during light-dark cycles, correlated with the acetate uptake. (D),(E),(F) measured H_2 production (blue circles). Constant low level H_2 was produced during continuous illumination and 16 h light cycles, but H_2 production strongly increased in each light period of the 8 h light cycles. (G),(H) PHAs fluorescent counts per gram biomass in the light/dark experiments. A PHAs peak was measured at the beginning of each light phase under the 16 h light conditions, however less clear pattern could be detected under the 8 h light experiments.